

ATMOSPHERIC IRON INPUTS AND PRIMARY
PRODUCTIVITY: PHYTOPLANKTON RESPONSES
IN THE NORTH PACIFIC

R.W. Young,¹ K.L. Carder,¹ P.R. Betzer,¹
D.K. Costello,¹ R.A. Duce,²
G.R. DiTullio,^{3,5} N.W. Tindale,²
E.A. Laws,³ M. Uematsu,^{2,6}
J.T. Merrill,² and R.A. Feely⁴

Abstract. As part of the Asian Dust Inputs to the Ocean System (ADIOS) project, atmospheric dust fluxes and primary productivity were monitored during the dusty season (spring) of 1986 at 26°N, 155°W, in the North Pacific Ocean. The arrival of major pulses of dust from Asia was followed by major increases in primary production. Extensive chemical analyses of the atmospheric particles showed that they were iron-rich (10-15%) and, further, that if only a small proportion (e.g. 10%) of this iron dissolved in the euphotic zone, it would be sufficient to support the

increases in carbon production at this location. The systematic increases in production noted with increasing depth and time may result from a continual release of iron from the settling particles in the euphotic zone. At all depths, systematic decreases in production followed the initial surge in production, indicating that the phytoplankton may have evolved from being iron-limited to being nitrogen-limited. Comparison of particle concentrations calculated by a particle settling model with primary productivity profiles indicated that mineral particles with settling velocities equivalent to those of 14 to 18- μ m-diameter spherical quartz particles were the most likely source for the iron stimulating the increases in primary production.

¹ Marine Science Department, University of South Florida, Saint Petersburg.

² Graduate School of Oceanography, University of Rhode Island, Kingston.

³ Department of Oceanography, University of Hawaii, Honolulu.

⁴ Now at Moss Landing Marine Laboratories, Moss Landing, California.

⁵ Now at Department of Marine Sciences and Technology, Hokkaido Tokai University, Sapporo, 005 Japan.

⁶ Pacific Marine Environmental Laboratory, NOAA, Seattle, Washington.

Copyright 1991
by the American Geophysical Union.

Paper number 91GB00927.
0886-6236/91/91GB-00927\$10.00

INTRODUCTION

A host of studies have investigated the dynamics of oceanic phytoplankton communities in an attempt to understand the principal factors that control their distribution, production, species composition, and variability in time and space [Goldman et al., 1979; Jackson, 1980; Marra, 1980; Ryther, 1969; Sharp et al., 1980; Sheldon et al., 1973; Venrick, 1982; Walsh, 1988]. It is clear that researchers do not yet have a complete understanding of the processes that control primary production nor of their relative

importance. Fundamental controls that are recognized as being of greatest importance include light, nutrients, grazing, temperature, and settling rates.

Some of the early work in the English Channel [Harvey, 1937] as well as that in the Sargasso Sea showed that the major nutrients (nitrate, phosphate, and silica) exerted important controls over phytoplankton populations [Menzel et al., 1963; Ryther and Guillard, 1959]. In particular, the experiments of Menzel and Ryther [1961] in the Sargasso Sea showed the marked response of natural phytoplankton populations to additions of nitrate, phosphate, silica, and iron. Iron has a particularly crucial biochemical role in the photosynthetic process and was cited by Harvey [1937] as being especially important for most of the open ocean, which is, by and large, iron-poor [Landing and Bruland, 1987]. While the relative importance of iron to oceanic phytoplankton communities remains unresolved, it has a depth distribution qualitatively similar to that of nitrate, phosphate, and silica [Martin and Gordon, 1988]. The primary source for the nanomolar quantities of iron in the mixed layer was, until recently, assumed to be from vertical inputs of deeper, iron-rich water [Bruland, 1983]. Duce [1986] showed that although the upward fluxes of nitrate and phosphate were sufficient to account for carbon production in the open ocean, the corresponding upward fluxes of iron were, given existing estimates of iron/carbon stoichiometric utilization ratios, insufficient. More to the point, he calculated that the atmospheric input of iron was sufficient to account for most of the iron dissolved in surface waters.

Recently, several papers have considered the possibility that iron may limit primary production over large reaches of the oligotrophic ocean [Martin and Gordon, 1988; Davies, 1990]. The culture experiments of Martin and co-workers [Martin and Fitzwater, 1988; Martin et al., 1989] with natural populations provide evidence that open-ocean species respond rapidly to small additions of iron and, further, that without additional iron, large open-ocean areas such as the Gulf of Alaska and the Southern Ocean around Antarctica, will continue to be characterized by high concentrations of nitrate and phosphate.

Studies of dust and CO₂ in ice cores from Antarctica suggest that today's ocean

is iron-limited. During glacial periods, iron-bearing atmospheric dust fluxes were higher and the partial pressures of CO₂ in the Earth's atmosphere were substantially lower [Delmas et al., 1980; De Angelis et al., 1987; Neftel et al., 1982] than they are at present or were during previous interglacial periods. Martin interprets the long-term Antarctic record as supporting the theory that productivity in (at least) the southern ocean is iron-limited and that changes in atmospheric CO₂ between glacial and interglacial periods are a result of variations in aeolian iron inputs (via dust) to this region. We have attempted to quantify the way(s) contemporary primary producers in the open ocean respond to inputs of iron-bearing dust.

In March and April 1986, investigators participating in the Asian Dust Inputs to the Ocean System (ADIOS) project observed the fluxes and fates of atmospherically derived mineral aerosols in the oligotrophic Pacific. During the 27-day sampling period, pulses of eolian material originating in Asia moved into our sampling site north of Hawaii at 26°N, 155°W [Betzer et al., 1988]. Measurements of primary production were made at the same time [Laws et al., 1987]. As far as the authors are aware, this is the first time that both atmospheric iron fluxes and primary production have been simultaneously measured in the open ocean. Since major dust inputs occurred during this sampling period (March-April 1986), the data set provides an opportunity to address the question of iron-stimulated production in the open ocean.

MATERIALS AND METHODS

Concentrations and fluxes of mineral particles were determined in the atmosphere and upper water column for a 27-day period in March-April 1986 at a station in the North Pacific (26°N, 155°W) aboard the R/V Moana Wave. Procedures for collection and analysis of atmospheric aerosols and total deposition samples for aluminum, an indicator of aluminosilicate materials, have been described previously [Betzer et al., 1988, and references therein]. Basically, a large polyethylene funnel with a 2-L polyethylene bottle suspended underneath was mounted at the top of a 10-m-high tower on the bow of the ship. Samples were collected every 2 days, or sooner if it rained, by rinsing down the

funnel and filtering the contents of the catchment bottle through 0.45- μm pore size Nucleopore filters. To ensure quantitative recovery of particles by the first rinse, a second rinse was checked for particles.

Mineral fluxes in the water column were estimated with free-drifting sediment traps, some of which were fitted with programmable sample changers which isolated a sample every 4 hours [Costello et al., 1989]. Traps were deployed at depths of 37, 127, 400, 900, 2200, and 3500 m.

Atmospheric and water-column samples were analyzed using computer-controlled scanning electron microscopy (SEM) and energy dispersive X ray analysis (EDXA). Each particle was measured (length and width) and then chemically analyzed for 5s. For consistency, particle size is expressed as the diameter of a volumetrically equivalent sphere. This volumetrically equivalent spherical diameter (ESD) is determined using the volume of the original particle calculated either as a prolate ellipsoid if the length:width ratio of the particle is $< 3:1$, or as a cylinder if length:width $\geq 3:1$ [see Carder et al., 1986]. Particles were ultimately tallied by ESD sizes and chemical classes as determined by relative proportions of Si, Al, Fe, Ti, Mg, and Ca.

The primary productivity studies were performed using the clean sampling and incubation techniques described by Laws et al. [1990]. In order to simulate light quality as well as quantity, light was attenuated in on-deck incubators with a combination of neutral density filters and blue and blue-violet Rohm and Haas Plexiglas filters (numbers 2069 and 2424, respectively). The incubators had visible light transmission levels of 100, 35, 18, 3.5, 1.0, and 0.1% of subsurface (0.5 m) photon fluxes. To determine the depths corresponding to these light intensities, photon fluxes in the water column were measured at local noon on the day after the ship arrived on station using a spherical quantum sensor (LiCor model 193SB) which was attached to a frame mounted on the top of a Seabird conductivity-temperature-depth (CTD) system. The CTD system was used to locate depths accurately and to provide hydrographic data. On-deck photon fluxes were simultaneously monitored with a LiCor model 190SB cosine-corrected quantum sensor. Outputs from both sensors were integrated for 1 min and submarine photon fluxes calculated as a fraction of surface photon fluxes by a LiCor model 1000 data

logger. The output from the deck-mounted sensor was integrated by the data logger from dawn to dusk to determine daily surface irradiance. Continuously flowing surface seawater was used to maintain the temperature in the incubators. On days that productivity was measured, the average in situ seawater temperature differential between surface and 150 m declined about 1.3°C.

All water samples were obtained using 30-L Teflon-coated Go-Flo bottles (General Oceanics) which had been rinsed with 1.5 N HCl (Baker, instra-analyzed). Hydrocasts were started at approximately 0400 local time, and incubations in 4.4 L polycarbonate bottles were begun just before sunrise with the addition of 1 mL of $\text{NaH}^{14}\text{CO}_3$ solution (specific activity of 15-25 Ci mol^{-1} , 500 mCi L^{-1}). All incubations lasted 24 hours and ^{14}C activity in all the sample bottles was measured by the addition of 0.5 mL of sample water to 0.2 mL of a 1:1 solution of phenethylamine:methanol [Iverson et al., 1976]. Total particulate ^{14}C activity was measured by filtering triplicate 100-mL sample aliquots onto Whatman GF/F glass fiber filters at sunset and after 24 hours. To drive off residual inorganic ^{14}C , the filters were stored in scintillation vials containing 1 mL of 10% HCl [Lean and Burnison, 1979; Goldman and Dennett, 1985]. A time zero blank was subtracted from all productivity samples in accordance with the recommendations of Morris et al. [1971]. Because nonphotosynthetic ^{14}C uptake may occur at very different rates in the light and dark [Hecky and Fee, 1981], dark bottles were not used as corrections for nonphotosynthetic processes (i.e., gross daylight productivity values are reported). Inorganic carbon concentrations were determined by titration [Strickland and Parsons, 1972]. Radioactivity measurements were made by liquid scintillation counting using an Aqueous Counting Scintillant (ACS from Amersham) as the fluor on a Searle Analytic Delta 300 liquid scintillation counter. Quench corrections were made using the external standard ratio. Activities were converted to uptake rates using the equations of Strickland and Parsons [1972].

A particle transport model was written to simulate the advection and diffusion of particles injected into the mixed layer during the study period. The raw input data consisted of individual SEM EDXA analyses for more than 60,000 eolian

particles collected at the sea surface during 615 hours of continuous sampling. The individual particle size data from the SEM EDXA were transformed into a smooth, continuous, mass-flux, input function using an Akima semispline fitting function [Ruckdeschel, 1981].

Particle-settling velocities w (centimeters per second) were determined for individual particles utilizing the shape-dependent Stokes settling equation [Lerman, 1979; Carder et al., 1986]. For a sphere the equation is

$$w = \frac{g \times (\rho_p - \rho_m) \times D^2}{18 \times \eta} \quad (1)$$

where g is the gravitational constant (cm s^{-2}); ρ_p and ρ_m are the densities (grams per cubic centimeter) of the particle and of the medium respectively; D is the diameter (centimeters) of the volumetrically equivalent sphere, and η is the molecular viscosity (grams per centimeter per second) of the seawater.

The individual particle densities were determined through elemental analysis using the SEM EDXA. Each particle was assigned to one of eight velocity classes representing particle settling velocities ranging from 2 to $154 \mu\text{m s}^{-1}$.

Particles in the mixed layer are subject to the physical processes of advection and eddy diffusion. To preclude artificial diffusion from occurring in the model, numerical stability must be obtained by requiring the time step t (seconds) and bin depth z (centimeters), together with particle-settling velocity w and eddy diffusion coefficient k ($\text{cm}^2 \text{s}^{-1}$) to meet the following requirements [Roache, 1982]:

$$-1 \leq (\pm)c/2 + d \leq 1 \quad (2)$$

where $c = wt/z$ is the Courant number and $d = kt/z^2$ is the diffusion number. The most restrictive form of the above inequality is

$$wt/z + 2kt/z^2 \leq 2 \quad (3)$$

In order to avoid errors due to numerical dispersion, we chose to set the left-hand side of the above inequality equal to 1. This yields the following time step:

$$t = [2k/(z^2) + w/z]^{-1} \quad (4)$$

This time step is simply the time it

takes for a particle to fall one sample bin distance in the absence of eddy diffusion. With eddy diffusion, the maximum transport distance for a particle in one time step is exactly equal to one sample bin distance. Also, eddy diffusion dominates advection when k exceeds the particle-settling velocity times one-half the bin depth.

A series of known input functions (delta, ramp, and transcendentals) were used to test the transportive and conservative properties of the model. With w and k set equal to and greater than 0, respectively, the various functions retained both their shapes and integrated numerical values. The three important properties of the model are that (1) the surface (upper boundary) is reflective with respect to both advection and diffusion (forward difference), (2) the bottom of the mixed layer (lower boundary) is reflective for diffusion (backward difference) but allows particles to advect through the boundary and out of the model space, and (3) the interior of the model allows centered difference diffusion and forward advection with depth and time [see Roache, 1982].

RESULTS AND DISCUSSION

According to routine meteorological reports from China, a major dust outbreak occurred in 1986 between March 15 and 17. Isentropic trajectory analyses at 300°K revealed that the large influxes of "giant" dust particles (greater than $100 \mu\text{m ESD}$) observed on the ship between March 26 and 31 (Figure 1a) came from northern China. These analyses also revealed that the transport from Asia to our study site required some 7 to 11 days [Betzer et al., 1988]. Prior to this event, a smaller outbreak occurred which caused an influx of high-iron content dust to our study area on March 23. This suggests that our study began just as the first significant influx of Asian dust for the month of March arrived at our station.

The influx of particles observed on April 6-8 (Figure 1a) were associated with trajectories having an intermittent Asian origin. A dust cloud observed on lidar profiles taken over Japan on 1 to 2 April (Y. Iwasaka, personal communication, 1987) is consistent with a trajectory reaching the study site on April 8. A small dust outbreak was observed in northern China on April 8, and isentropic analyses indicate that it was the source of the fine aerosols

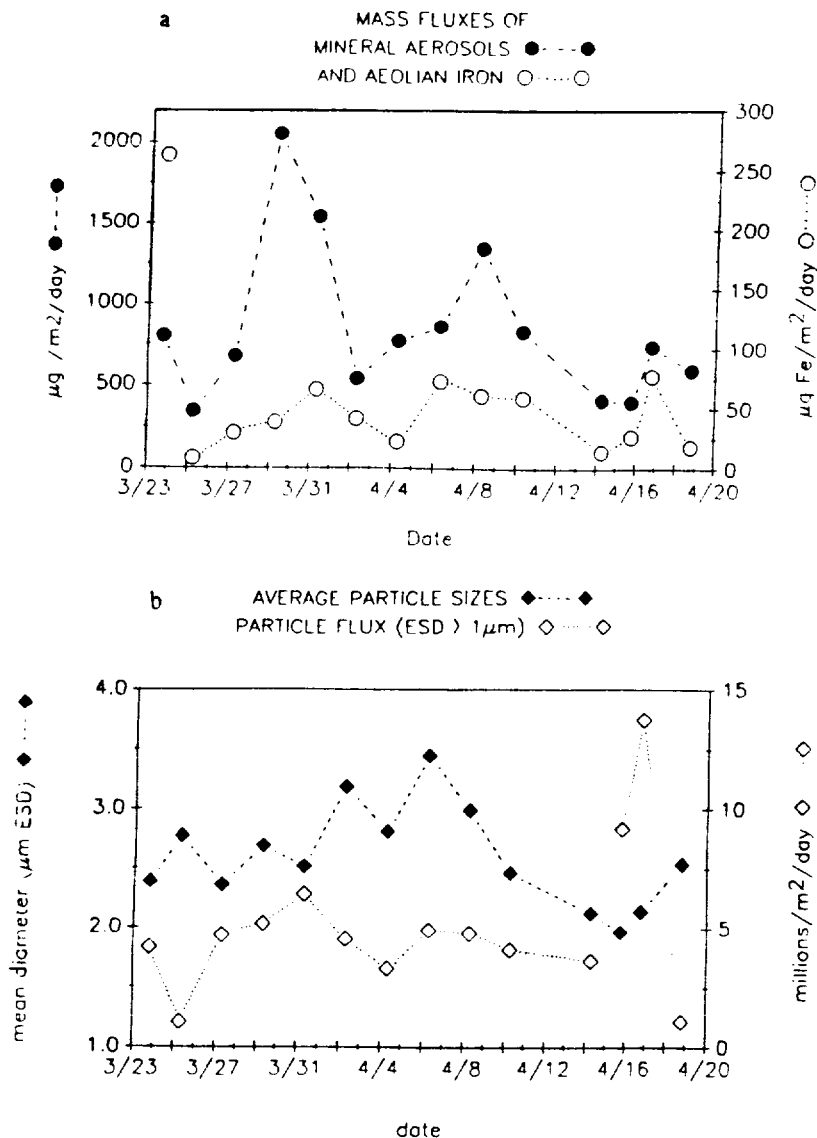


Fig. 1. Particle flux and size as a function of time for spring 1986 at 26°N, 155°W: (a) mineral aerosol mass flux and particulate iron mass flux; and (b) mean particle diameters and numerical flux of mineral particles larger than 1-μm area-equivalent diameter.

reaching our ship on April 16-17 (Figures 1a and 1b).

The average daily wind speed during the study (Figure 2) corresponded rather well with the flux of fine dust (<25 μm ESD) to the sea surface (not shown in Figure 1). A correlation coefficient of $r^2 = 0.73$ was found between the mass fluxes of 15 dust samples and wind speeds averaged over the particle collecting intervals. During the late March and April influx periods, significant increases in wind speed

accompanied the arrival of dust-laden fronts. Between April 7 and 11, winds were high enough to cause a complete cessation of sediment trap deployment and retrieval activities.

The high-wind events, while delivering iron-rich dust to the study site (Figure 1a), also influenced the density structure of the water column. After March 22 the water column was homogenous from the surface to 120 m. The calm, sunny period on March 24-25 stratified the upper 10 m,

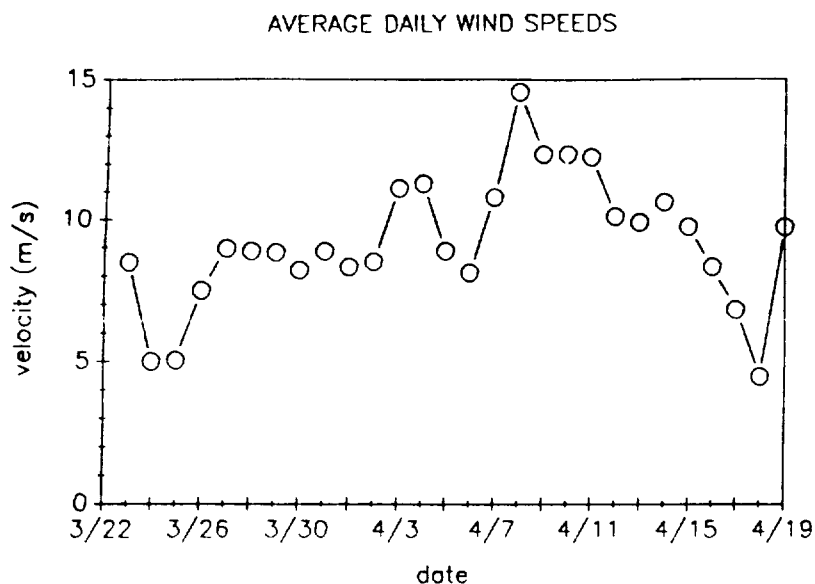


Fig. 2. Daily average wind speed (meters per second) for the 1986 ADIOS expedition.

but a cold front on March 26 rehomogenized the upper water column. Some stratification below 40 m gradually became apparent after March 29, but the water column again became thoroughly mixed to 120 m by April 8. The profiles remained homogenous until April 16, when stratification in the top 10 m due to solar heating became apparent.

The major dust influx events (March 26-31, April 6-8, and April 16-17) consisted of aerosols having markedly different characteristics (Figures 1a and 1b). The event beginning on March 26 provided "giant" particles greater than 100 μ m ESD [see Betzer et al., 1988]. In contrast, particles that were deposited between April 6 and 8 contained no such "giants," even though they were associated with the front that produced the highest wind velocities observed during the study. The number of particles (Figure 1b) collected on April 17 when wind velocities (Figure 2) decreased to minimum values was over $13 \times 10^6 \text{ m}^{-2} \text{ d}^{-1}$. This was more than twice the number of particles collected during the March 26-31 event, although the mass flux was much less due to the smaller size of the particles.

Aerosol deposition samplers depend on unimpeded particle settling to collect unbiased samples. Since fine particles settle much more slowly than larger ones do and are more susceptible to advection and eddy diffusion processes, the collection efficiency of these samplers depends on

both the particle size distribution in the atmosphere and wind velocity. For these reasons, particle distributions in the various samples may not always be directly comparable to one another. However, they represent the best measure of the actual flux of particles to the ocean surface.

The marked difference in the size of deposited particles within and between events also affects the distribution of particles with depth in the water column over time, and the relative availability of iron and other minor nutrients associated with particle surfaces. Since dissolution occurs at particles surfaces, we compared the iron mass flux to the surface area flux for various size classes of atmospheric particles collected during the study (Figure 3). The resulting curve suggests that over the entire study period, iron is most available for dissolution from the 8- μ m-ESD size class. While particles smaller than 8 μ m ESD have larger ratios of surface area to volume, their total contribution was just over 20% of the total aerosol iron flux to the ocean during this study. This was due to both their lower iron content and smaller mass flux (see Table 1).

A quartz-equivalent spherical diameter (QESD) is similar to an ESD except that the volume of the sphere from which the diameter is calculated is adjusted by the density of the original particle to yield an equivalent quartz sphere of density 2.65

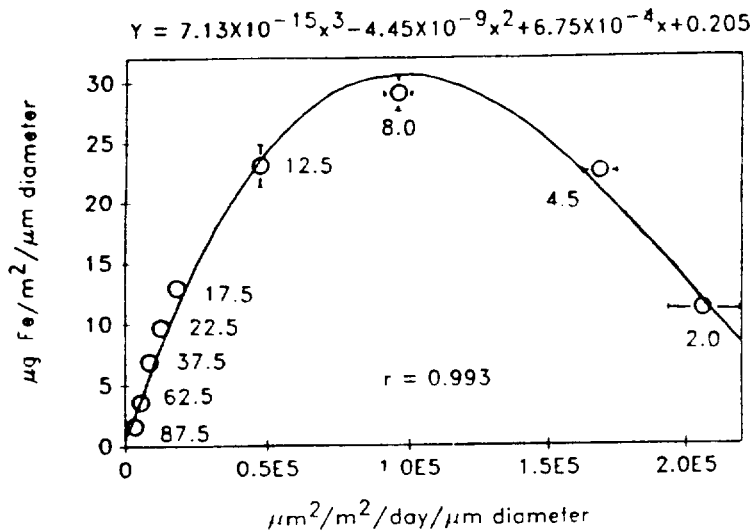


Fig. 3. Atmospheric iron flux versus the flux of total particulate surface area to the study site for various particle size classes based upon analysis of 60,000 mineral particles collected during ADIOS. The third-order regression equation shown fits the data with a correlation coefficient better than 0.99. Points are labeled with the middle diameter (μm) of the size classes.

g cm^{-3} that has the same settling velocity as the particle. This transformation is useful to simplify the description of the settling velocity classes discussed in this paper.

Particles in the 7 to 22- μm -QESD size range averaged more than 12% iron, while the 11 to 14- μm -QESD class consisted of 15.5% iron (see Table 1). Because of the large mass flux in the 14 to 18- μm -QESD range, this class provided the greatest influx of iron to the ocean during ADIOS. While these calculations represent averages over the entire 27-day study period, the

contributions from individual 2-day collections varied significantly in particle composition (e.g., density, mineralogy, and shape) and size [see Betzer et al., 1988]. The effect of each of these variations on particle settling speed is included as input data for the particle dynamics model that is discussed below.

In terms of transporting iron and other trace metals to depth, the larger-QESD particles have the greatest settling velocities. Conversely, these particles have the shortest residence time in the euphotic zone, permitting less time for

TABLE 1. Average Daily Particulate Mass and Iron Fluxes of Mineral Aerosols Collected Between March 22 and April 19 at 26°N, 155°W, by Quartz Equivalent Spherical Diameter (QESD) Size Classes

	QESD, μm								
	<1	1-3	3-5	5-7	7-9	9-11	11-14	14-18	18-22
Mass Flux	0.74	4.30	8.97	12.22	13.74	17.0	20.67	30.48	23.48
Percent Fe	5.5	9.4	10.6	9.7	12.1	11.4	15.5	13.0	12.9
Fe flux	0.04	0.40	0.95	1.19	1.66	1.94	3.20	3.96	3.03

Fluxes are in $\mu\text{g m}^{-2} \text{d}^{-1}$. For larger particles, see Betzer et al. [1988].

dissolution processes to remove iron. Thus the unknown ratio of settling to dissolution rate will play an important role in determining which size class provides the most dissolved iron to the euphotic zone and where within the euphotic zone that iron becomes available.

Vertical mixing will also have a smaller relative effect on the distribution of the larger particles except perhaps during the most severe wind events associated with frontal passages. We can gain some insight into the dissolution rate question by observing the response of phytoplankton growth rates during the deposition of iron-rich mineral aerosols at our North Pacific site.

The response of the phytoplankton to rapid-mixing events followed by large influxes of dust at the surface can be illustrated in a number of ways. The correlation coefficient r^2 between primary production and wind speed was 0.82 ($n=6$), close to that for the influx of fine dust (<25 μm ESD) versus wind speed averaged over the aerosol collection interval, which again is $r^2 = 0.73$ for $n=15$. Only fractions finer than 25 μm ESD are considered in this calculation because large, iron-poor particles would probably settle through the euphotic zone too rapidly to release enough iron to significantly enhance primary productivity.

The primary productivity data in Table 2 can be used to calculate iron demand by phytoplankton for comparison with eolian iron availability (Figure 4). Allowing an average of 4 days for the phytoplankton to

respond to the iron input from mineral aerosols and assuming 10% of the eolian iron influx dissolves [Moore et al., 1984] within the euphotic zone provides the best agreement between "iron availability" and "planktonic stoichiometric iron demand" integrated over the euphotic zone. This "demand" is based upon estimating the iron required to support the observed growth assuming the minimum Fe:C requirement (1:130,000) found in laboratory studies for a coastal phytoplankton species [Anderson and Morel, 1982].

An evaluation of the fraction of particulate iron dissolved during the 7 days required for an 8- μm -ESD mineral particle to settle into a sediment trap at 37 m depth was carried out by comparing the iron content of aerosols (10%) collected with our shipboard sampling tower to those observed in the sediment trap (8%). In both cases the analyses were carried out on particles in the 6 to 10- μm class and restricted to those whose chemical signatures (SEM EDXA) linked them to the atmosphere. This 2% reduction in the particulate iron fraction suggests that roughly 20% of the iron associated with mineral aerosols dissolved in natural seawater in 7 days. This is within the range of iron dissolution values determined by Moore et al. [1984] and subsequently expanded by Maring and Duce [1987], and Zhuang et al. [1990], who found that 10-50% of aerosol iron dissolves in seawater.

One novel way to estimate the atmospheric flux of soluble iron to the ocean may be through the use of atmospheric

TABLE 2. Primary Productivity by Depth and the Integrated Total to 150 m at 26°N 155°W During ADIOS

	Depth, m					
	March 25	March 29	April 1	April 4	April 6	April 14
0	3.94	1.55	2.44	3.46	3.50	3.19
20	3.68	5.32	4.15	3.77	4.60	5.12
40	3.02	4.10	3.48	3.18	3.64	4.21
80	3.05	2.86	4.01	4.70	3.78	6.25
100	3.00	2.18	3.11	6.60	3.89	4.06
150	0.35	0.77	0.30	0.54	1.09	0.27
Total	372	426	449	591	513	605

Depth data are in $\text{mg C m}^{-3} \text{d}^{-1}$. Total data are in $\text{mg C m}^{-2} \text{d}^{-1}$.

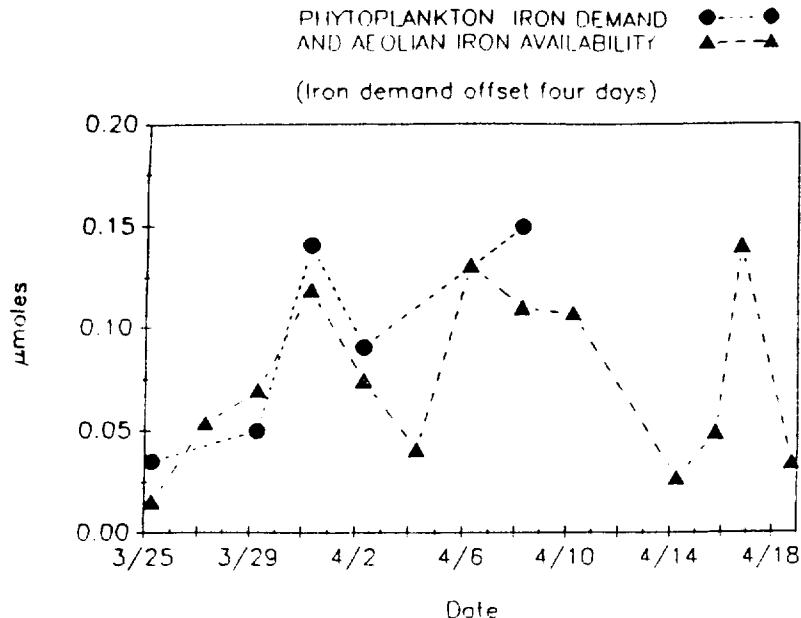


Fig. 4. Stoichiometric iron demand by phytoplankton required to support the increase in productivity noted, compared with eolian iron availability during ADIOS. The iron availability curve exhibits a 4-day phase lag relative to mineral aerosol collections made on the ship.

^{210}Pb fluxes. Turekian and Cochran [1981] and Turekian et al., [1989] combined the $\text{Al}/^{210}\text{Pb}$ ratio measured in aerosol samples with the measured ^{210}Pb flux to obtain an estimate of the atmospheric Al flux to the ocean in the North Pacific. From comparison of this calculated flux with a directly measured Al flux, it was observed that the calculated flux was less than the measured total Al flux but was similar to the flux of Al which would dissolve in the ocean. The reason for this is unclear, but it may apply to iron as well, although it is known that the iron present in mineral aerosols is considerably more soluble than the aluminum [Zhuang et al., 1990; Maring and Duce, 1987].

In short-term (2 hour) reaction experiments with mineral aerosols in seawater (pH 8), Moore et al. [1984] found that 10% of the particle-associated iron dissolved relative to aluminum, which was assumed to be insoluble. Later, Maring and Duce [1987] found that 5-10% of the aluminum dissolves, resulting in a larger fraction of the particulate iron (15-20%) dissolving than was indicated by Moore. These experiments dealt with aerosols from the maritime Atlantic which are distinct from

those being transported into the North Pacific from Asia. Nonetheless, transit times for the iron-rich atmospheric particulates moving through the euphotic zone of the North Pacific (transit times ranging from over 600 hours for 9- μm particles to over 100 hours for 22- μm particles) provide at least 50 times longer for dissolution processes (100 hours versus 2 hours) than was permitted in the above experiment. In addition, these mineral aerosols were transported in the atmosphere with corrosive, fine-mode acid sulfates (Clarke et al. [1987] and references cited by Zhuang et al. [1990]). Thus aerosol iron was probably immersed in essentially a sulfuric acid solution during its transport across the North Pacific. The strong acid would have had a week or more to dissolve the iron, making it considerably more labile than it was when it started its journey in China.

In their study of aerosol-seawater interactions, Zhuang et al. [1990] found that dissolved iron concentrations increased to saturated equilibrium concentrations of 10-20 nmol per kilogram seawater in just a few minutes. Once these concentrations were reached, relatively

little additional iron dissolved. Therefore, it may not be possible to say that a certain percentage of particulate iron dissolves without knowing the total iron concentration in seawater.

On the basis of these studies, it appears that particles settling through the euphotic zone dissolve iron from their surfaces at rates dependent on the deficit in the equilibrium concentration, which may be a function of the assimilation rate of phytoplankton at various depths. The eolian particles, when present in sufficient quantities, may thus be acting as mobile reservoirs of iron that continuously provide enough dissolved iron to maintain equilibrium concentrations of 10-20 nmol kg⁻¹ in the upper water column. This may explain how the iron can be both readily available for dissolution and continuously available throughout the euphotic zone.

It seems likely then that at least 10% of the mineral aerosol iron associated with the Asian dust dissolves in the euphotic zone of the North Pacific. While the calculations described above are simplistic, they do suggest that even after settling to the base of the euphotic zone (settling times between 4 and 25 days), aerosols could still provide iron to phytoplankton.

The increase in primary productivity values leave little doubt that nitrogen was available to primary producers even though it was typically less than 0.2 µg-at.L⁻¹ in the top 100 m (data published by DiTullio and Laws [1991]). The exception is on April 4 when the NO₃⁻ concentration averaged 0.43 µg-at.L⁻¹ in the top 40 m, with a maximum value at the surface of 0.67 µg-at.L⁻¹. At the productivity rate

measured in our study area, DiTullio and Laws [1991] calculated that this was enough N to provide for 5.8 days of new production in the upper 40 m of the euphotic zone. The substantial decrease in NO₃⁻ concentration between the surface and 100 m, $\delta\text{NO}_3^- = 0.42 \text{ } \mu\text{g-at.L}^{-1}$, suggests that rather than being upwelled during wind-induced mixing, nitrogen oxides were delivered to the sea from the atmosphere. By April 6, average NO₃⁻ concentrations in the upper 100 m decreased to 0.15 µg-at.L⁻¹, and on April 14, they averaged 0.08 µg-at.L⁻¹.

Eolian phosphorous fluxes were estimated using the individual particle analysis data from the SEM EDXA system. Stoichiometric calculations using these data suggest that even if 100% of the eolian phosphorous dissolved, less than 1% of the observed primary production could have been supported. Thus dust-borne phosphorous by itself cannot explain the changes in primary production that were observed with time and depth.

Figure 5 is a two-dimensional plot of the primary production values in Table 2 ranked by depth. From contours drawn around the top three ranks it is clear that growth rates are enhanced in a systematic fashion, starting in near-surface waters and moving in time toward the base of the euphotic zone. The diagonal contour starting on March 25 can be interpreted as a productivity response to the large iron input measured on March 23 (Figure 1a). Although we sampled only the tail end of this event, the iron content of the mineral aerosol flux was nearly 35% (Figure 1a) making it the highest measured. In addition, 16% of this iron was transported by particles in the 14 to 18-µm-class, which could perhaps explain the well-

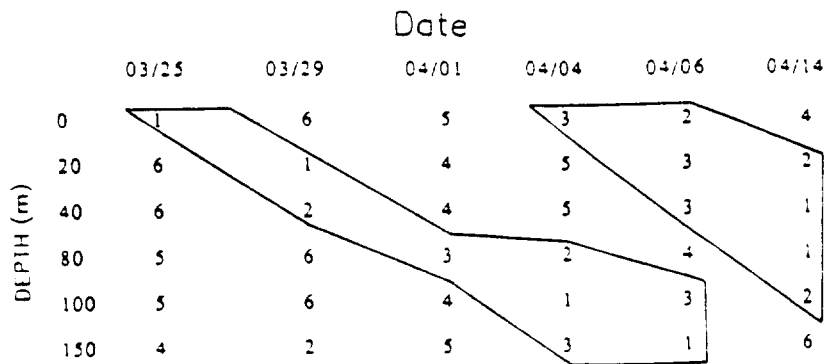


Fig. 5. A two dimensional plot of the primary production values in Table 2 ranked by depth.

defined nature of the growth enhancement contoured in Figure 5. This trend in phytoplankton response is consistent with iron dissolution from settling particles with a QESD of about 14 μm and a lag of 3 to 4 days before significant increases in growth are observed.

The next two iron input events (March 31 and April 6; see Figure 1a) appear to have combined together to produce a more prolonged productivity enhancement throughout the euphotic zone (Figure 5; April 4, 6 and 14). The initial productivity response to the March 31 event occurs in the surface sample taken at 0400 on April 4. By April 14 it had mixed with iron deposited during the April 6 event to create a broad band of high productivity extending from 20 to 100 m deep. This generated the highest integrated primary productivity measured during this study, 605 $\text{mg C m}^{-2} \text{d}^{-1}$ (see table 2). The divergent contour of the productivity enhancement caused by these events precludes making a similar estimate of the QESD of the particles responsible for it. However the next section considers the results of a particle dynamics model that more precisely defines particle trajectories in the water column from the aerosol deposition data.

In general, the sequence of increasing primary productivity down the water column is not consistent with mixing nutrient-rich water into the lower portion of the euphotic zone. In such a case we would expect to see the producers which are nearest the nutrient source respond first (i.e., those at about 100 m). The systematic depth-time responses noted in the North Pacific are consistent with an iron-limited system that initially responds to the iron released from mineral aerosols settling through the water column. Of course, if nitrogen enrichment is also provided by aerosol influxes [DiTullio and Laws, 1991], a similar pattern could evolve. However, most aerosol N enrichment would be expected to occur rapidly near the sea surface and not be distributed to depth over time in the nondiffusive manner suggested by Figure 5.

It is interesting to note that the enhancements in primary productivity found between 40 m and 100 m were relatively brief events. After reaching a peak on April 4, for example, productivity at 100 m decreased over 40% by April 6, suggesting productivity was being limited. This decrease could hardly have been due to a

light limitation since the productivity at 150 m for the same period showed a 100% increase. It is possible that the supply of atmospheric iron at 100 m was exhausted by this time, thus making it the limiting factor. However, it is also plausible that the system responded to the atmospheric iron to the extent possible and in so doing evolved from being iron-limited to being nitrogen-limited. The question involving such a transformation in the euphotic zone will be explored in the following section.

MODEL RESULTS

Results of calculations using a particle dynamics model are only presented for particles in the 9 to 22- μm -diameter range of the size classes shown in table 1. Larger particles reside in the euphotic zone only for a period less than 3.5 days [see Betzer et al., 1988]. They also have smaller values for factors important to dissolution kinetics, e.g., iron content and ratios of surface area to volume (see Figure 3). Particles smaller than 9 μm QESD settle slowly enough that their fall velocity would transport them to depths less than about 30 m in approximately 6 days. Thus any iron dissolved from this size class would largely be restricted to the upper portion of the euphotic zone.

To calculate the concentration of particles at any depth, combined fluxes due to settling and diffusion were modeled. This required that each particle analyzed by SEM EDXA be characterized in terms of length, width, area, and mineralogy (inferred from elemental chemistry) using the methods described by Carder et al. [1986]. The particle mass was obtained by multiplying the density appropriate to a given mineral class by the volume derived by either (1) assuming prolate ellipsoids of revolution for particles with length:width ratios shorter than 3:1, or (2) assuming a cylindrical form for particles with longer ratios. Settling velocities were then calculated with the equations provided by Lerman [1979], and the entire population for any collection was separated into nine different settling classes.

Because any given settling velocity class may contain particles with density values ranging from ca. 2.6 to 5.2 g cm^{-3} , we have chosen to present the results in terms of quartz-equivalent-spherical (QES) volume and diameters. Since most of the settling classes contain 10 to 15% iron by

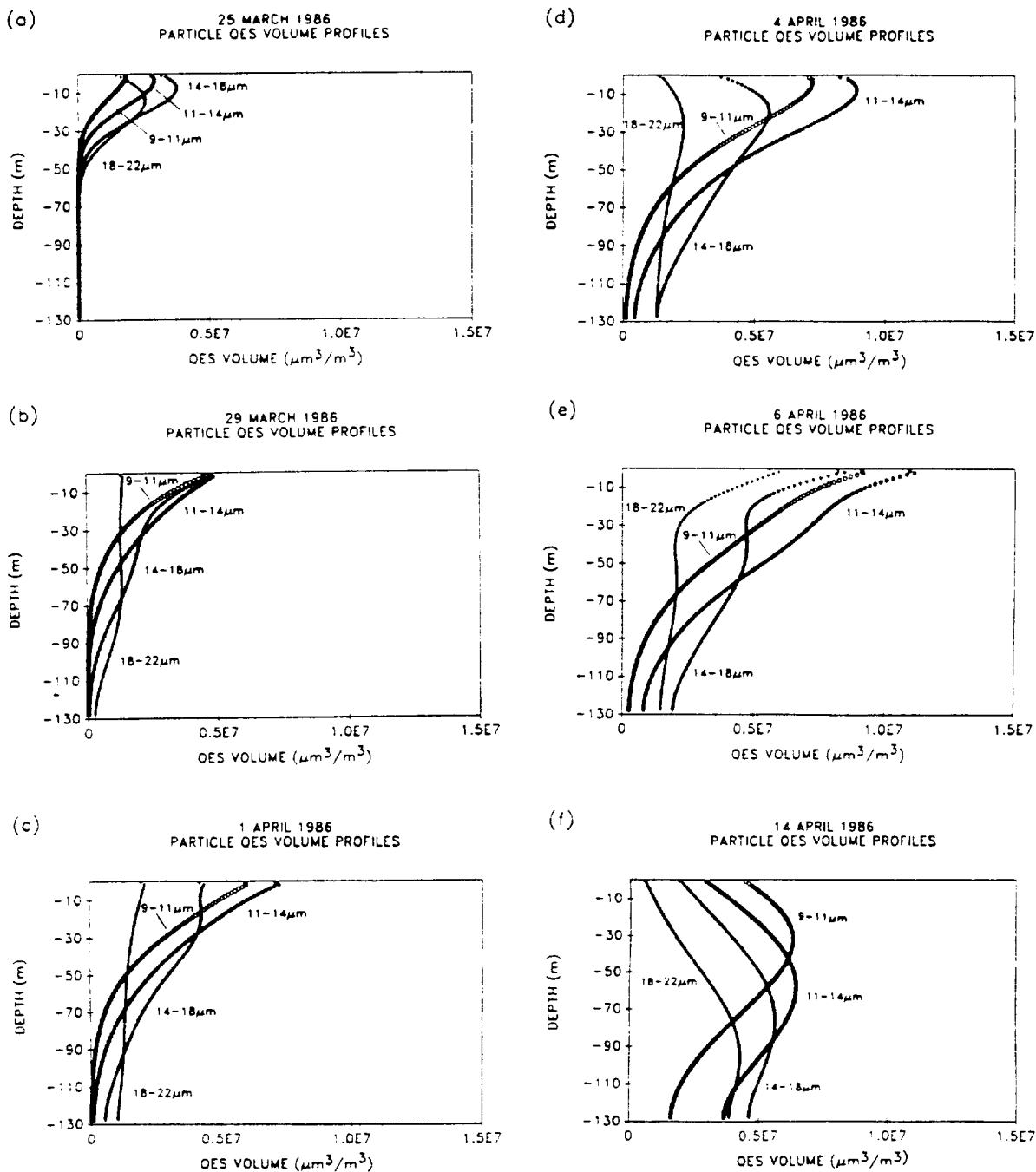


Fig. 6. Model-derived concentration profiles with depth for particles in various settling classes: (a) March 25, (b) March 29, (c) April 1, (d) April 4, (e) April 6, (f) April 14. The eddy diffusion coefficient for the simulation results is $10 \text{ cm}^2 \text{ s}^{-1}$.

mass, a convenient way to estimate the particulate iron availability at any depth is to multiply the QES volume concentration by the density of quartz (2.65 g cm^{-3}) and by 0.1.

Model-derived particle concentrations as a function of depth and time are shown in Figure 6. The water column at the study site was generally well-mixed down to 120 m with a viscosity of 1.05 cP and a density

of 1.02 g cm^{-3} . The vertical eddy diffusion coefficient k was assumed to be $10 \text{ cm}^2 \text{ s}^{-1}$ for the study period. Eddy diffusion coefficients as small as $k = 1 \text{ cm}^2 \text{ s}^{-1}$ did not significantly change the dispersal patterns for particles larger than about $14 \text{ }\mu\text{m}$ diameter.

The data shown in Figure 6 include only those particles reaching the sea surface after March 22. While we have no certain knowledge of the atmospheric fluxes prior to our study, dust reports from China suggest that no major influxes of dust from that source occurred earlier in the month. The temporal sequence of panels selected for display in Figure 6 corresponds to the dates when primary productivity measurements were made (e.g. see Table 2). The availability of mineral particles in various settling classes as a function of depth will be discussed relative to the measured biological response.

Using a concentration value $10^6 \text{ }\mu\text{m}^3 \text{ m}^{-3}$ as a marker of "earliest availability" for iron at a given depth, iron in the 14 to 18- μm class became available at 35 m on March 25, at 80 m on March 29, at 105 m on April 1, and well below 120 m by April 4 (Figure 6). The 18 to 22- μm class proceeded more quickly to depth, but was neither as abundant (Figure 6) nor as iron-rich (see Figure 3). The time period between "earliest availability" of iron at depth and detection of significant enhancements in productivity was about 3 to 4 days.

Comparing Figure 6 with Table 2, it is apparent that the time lags between the influx of the 14 to 18- μm class through the air-sea interface on March 23 and the observation of increased productivity at depth were 6 days at 40 m and 8 days at 80 to 100 m. In both cases, maximal productivity occurred three days after the 14 to 18- μm class first arrived at these depths. Total water column primary production increased over 30% between April 1 and 4 after (1) iron from the March 29 influx (see Figure 1a) had stimulated production at the surface, (2) productivity between 20 and 40 m was not yet severely limited by lack of nutrients [DiTullio and Laws, 1991], and (3) productivity between 80 and 100 m was stimulated by iron that had reached these depths from the March 23 influx (Figure 6d). Note that the highest primary productivity for the entire study occurred at 100 m on April 4 (Table 2). However, mixing across the nutricline was probably inadequate after April 4 to

support this maximum growth rate, causing a drastic decrease in productivity at 100 m on April 6. Since Figure 6e shows iron-bearing aerosols were abundant at this depth and time, it is likely that nitrogen limitation was responsible for this decline. The major wind event of April 7-11 (see Figure 2) reversed this trend by bringing deeper, nutrient-enriched water into the euphotic zone and transporting additional iron to the study area (see Figure 1a). Recall that by April 8 the top 120 m of the water column had been homogenized.

By April 14 a wide range of sizes of iron-bearing mineral aerosols were distributed throughout the euphotic zone (Figure 6f) resulting in the highest integrated total water column production for the study. The integrated primary productivity on this date was $605 \text{ mg C m}^{-2} \text{ d}^{-1}$, an increase of over 60% from the first sample taken 20 days earlier (Table 2). This large increase resulted from the significant productivity increases between 20 m and 100 m which are consistent with the prior passage through these depths of high concentrations of particles in the 14 to 18- μm -QESD size class. Iron from smaller particles in the 11 to 14- μm and 9 to 11- μm -QESD classes probably continued to support primary producers until major nutrient limitation became a factor in their growth response to the eolian inputs.

In summary, four distinct periods were delineated at our site in the north-central Pacific gyre: (1) a brief period when we first arrived on station when primary production was, by and large, limited by the availability of iron; (2) a period when primary production was stimulated by iron-rich, mineral aerosols settling through the mixed layer; (3) a period when this iron-enhanced production probably drove the system to nutrient limitation; and (4) a period during the last part of the cruise (April 7 to 16) when a combination of dust inputs and wind-driven mixing provided both sufficient iron and nutrients to support the highest primary production measured throughout the water column during this cruise.

CONCLUSIONS

1. During a period of high influxes of atmospheric dust (March-April 1986) to the north Pacific Ocean (26°N , 155°W), primary production increased more than 60%.

2. Increases in productivity were first

observed near the surface; subsequently, they were noted at ever increasing depths in the euphotic zone. The increase in productivity at a given depth followed the model-derived arrival time of iron-rich particles in the 14 to 18- μm -QESD settling class, implicating iron-rich settling particles in stimulating increased primary production.

3. The systematic shifts in primary production with depth and time suggest that when the iron-rich dust first arrived, the primary producers were iron-limited, and subsequently, primary productivity was stimulated to the extent possible before it was probably limited by other nutrients.

4. The observed increases in primary production can be explained by the dissolution of only 10% of the iron associated with the mineral aerosols that were deposited during the study.

Acknowledgments. The officers and crew of the R/V Moana Wave and the personnel of the University of Hawaii Marine Research Center did an excellent job of facilitating this work. We especially note the superb efforts of Captain W. Leonard, Deck Technician Curtis See, and Van Chisholm. We appreciate the help from the National Center for Atmospheric Research Computer Facility. This work was supported by grants from the NSF to the University of South Florida, the University of Rhode Island, and the University of Hawaii. The National Oceanic and Atmospheric Administration, through their PMEL facility, and the Office of Naval Research also supported this research.

REFERENCES

- Anderson, M. A., and F. M. M. Morel, The influence of aqueous iron chemistry on the uptake of iron by the coastal diatom Thalassiosira weissflogii, Limnol. Oceanogr., 27, 789-813, 1982.
- Betzer, P. R., et.al., Long-range transport of giant mineral aerosol particles, Nature, 336, 568-571, 1988.
- Bruland, K. W., Trace elements in sea water, in Chemical Oceanography, vol. 8, edited by J. P. Riley and R. Chester, pp. 157-220, Academic, San Diego, Calif., 1983.
- Carder, K. L., R. G. Steward, P. R. Betzer, D. L. Johnson, and J. M. Prospero, Dynamics and composition of particles from an aeolian input event to the Sargasso Sea, J. Geophys. Res., 91, 1055-1066, 1986.
- Clarke, A. D., N. C. Ahlquist, and D. S. Covert, The Pacific marine aerosol: Evidence for natural acid sulfates, J. Geophys. Res., 92, 4179-4190, 1987.
- Costello, D. K., K. L. Carder, P. R. Betzer, and R. W. Young, In situ holographic imaging of settling particles: Applications for individual particle dynamics and oceanic flux measurements, Deep Sea Res., 36, 1595-1605, 1989.
- Davies, A. G., Taking a cool look at iron, Nature, 354, 114-115, 1990.
- De Angelis, M., N. I. Barkov, and V. N. Petrov, Aerosol concentrations over the last climatic cycle (160 kyr) from an Antarctic ice core, Nature, 325, 318-321, 1987.
- Delmas, R. J., J. M. Ascencio, and M. Legrand, Polar ice evidence that atmospheric CO₂ 29,000 BP was 50% of the present, Nature, 282, 155-157, 1980.
- DiTullio, G. R. and E. A. Laws, Impact of an atmospheric oceanic disturbance on phytoplankton community dynamics in the North Pacific Central Gyre, Deep Sea Res., In press, 1991.
- Duce, R. A., The impact of atmospheric nitrogen, phosphorus, and iron species on marine biological productivity, in The Role of Air-Sea Exchange in Geochemical Cycling, edited by P. Buat-Menard, pp. 497-529, D. Reidel, Norwell, Mass., 1986.
- Goldman, J. C., J. J. McCarthy, and D. G. Peavey, Growth rate influence on the chemical composition of phytoplankton in oceanic waters, Nature, 279, 210-215, 1979.
- Goldman, J. C., and M. R. Dennett, Susceptibility of some marine phytoplankton species to cell breakage during filtration and post-filtration, J. Exp. Mar. Biol. Ecol. 86, 47-58, 1985.
- Harvey, H. W., The supply of iron to diatoms, J. Mar. Biol. Assoc., U.K., 22, 205-219, 1937.
- Hecky, R. E., and E. J. Fee, Primary production and rates of algal growth in Lake Tanganyika, Limnol. Oceanogr., 26, 532-547, 1981.
- Iverson, R. L., H. F. Bittaker, and V. B. Myers, Loss of radiocarbon in direct use of Aquasol for liquid scintillation counting of solutions containing ¹⁴C-NaHCO₃, Limnol. Oceanogr., 21, 756-758, 1976.
- Jackson, G. A., Phytoplankton growth and

- zooplankton grazing in oligotrophic oceans, Nature, 284, 439-441, 1980.
- Landing, W. M., and K. W. Bruland, The contrasting biogeochemistry of iron and manganese in the Pacific Ocean, Geochim. Cosmochim. Acta, 51, 29-43, 1987.
- Laws, E. A., G. R. DiTullio, and D. G. Redalje, High phytoplankton growth and production rates in the North Pacific subtropical gyre, Limnol. Oceanogr., 34, 905-918, 1987.
- Laws, E. A., G. R. DiTullio, K. L. Carder, P. R. Betzer and S. Hawes, Primary production in the deep blue sea, Deep Sea Res., 37, 715-730, 1990.
- Lean, D. R. S., and B. K. Burnison, An evaluation of errors in the ^{14}C method of primary production measurement, Limnol. Oceanogr., 24, 917-928, 1979.
- Lerman, A., Geochemical Processes in Water and Sediment Environments, John Wiley, New York, 481 pp., 1979.
- Maring, H. B., and R. A. Duce, The impact of atmospheric aerosols on trace metal chemistry in open ocean surface seawater, 1, Aluminum, Earth Planet. Sci. Lett., 84, 381-392, 1987.
- Marra, J., Vertical mixing and primary production, in Primary Productivity in the Sea, Environ. Sci. Res., vol. 19, Bookhaven Symp. Biol., vol. 31, edited by P. Falkowski, pp. 121-138, Plenum, New York, 1980.
- Martin, J. H., and S. E. Fitzwater, Iron deficiency limits phytoplankton growth in the northeast Pacific subarctic, Nature, 331, 341-343, 1988.
- Martin, J. H. and R. M. Gordon, Northeast Pacific iron distributions in relation to phytoplankton productivity. Deep Sea Res., 35, 177-196, 1988.
- Martin, J. H., R. M. Gordon, S. E. Fitzwater, and W. W. Broenkow, VERTEX: Phytoplankton/iron studies in the Gulf of Alaska, Deep Sea Res., 36, 649-680, 1989.
- Martin, J. H., R. M. Gordon, and S. E. Fitzwater, Iron in Antarctic waters, Nature, 345, 156-158, 1990.
- Menzel, D. W., and H. J. Ryther, Nutrients limiting the production of phytoplankton in the Sargasso Sea, with special reference to iron, Deep Sea Res., 7, 276-281, 1961.
- Menzel, D. W., E. M. Hulbert, and J. H. Ryther, The effects of enriching Sargasso seawater on the production and species composition of the phytoplankton, Deep Sea Res., 10, 209-219, 1963.
- Moore, R. M., J. E. Milley, and A. Chatt, The potential for biological mobilization of trace elements from aeolian dust in the ocean and its importance in the case of iron, Oceanol. Acta, 7, 221-228, 1984.
- Morris, I., C. M. Yentsch, and C. S. Yentsch, Relationship between light CO_2 fixation and dark CO_2 fixation by marine algae, Limnol. Oceanogr., 16, 854-858, 1971.
- Neftel, A., H. Oeschger, J. Schwander, B. Stauffer, and R. Zumbunn, Ice core sample measurements give atmospheric CO_2 contents during the past 40,000 years, Nature, 295, 220-223, 1982.
- Roache, P. J., Computational Fluid Dynamics, Hermosa, Albuquerque, N. Mex., 434 pp., 1982.
- Ruckdeschel, F. R., Basic Scientific Subroutines, vol. 2, McGraw Hill, New York, pp. 305-310, 1981. Ryther, J. H., Photosynthesis and fish production in the sea, Science, 166, 72-76, 1969.
- Ryther, J. H., and R. R. L. Guillard, Enrichment experiments as a means of studying nutrients limiting to phytoplankton production, Deep Sea Res., 6, 65-69, 1959.
- Sharp, J. H., M. J. Perry, E. H. Renger, and R. W. Eppley, Phytoplankton rate processes in the oligotrophic waters of the central North Pacific Ocean, J. Plankton Res., 2, 335-353, 1980.
- Sheldon, R. W., W. H. Sutcliffe, and A. Prakash, The production of particles in the surface waters of the ocean with particular reference to the Sargasso Sea, Limnol. Oceanogr., 18, 719-733, 1973.
- Strickland, J. D. H., and T. R. Parson, A practical handbook of seawater analysis, 2nd ed., Bull. Fish. Res. Board Can. 167, Ocean, Bioscience, 36, pp. 251-257, 1972.
- Turekian, K. K. and J. K. Cochran, ^{210}Pb in surface air at Enewetak and the Asian dust flux to the Pacific, Nature, 292, 522-524, 1981. (Correction, Nature, 294, 670, 1981.)
- Turekian, K. K., W. C. Graustein, and J. K. Cochran, Lead-210 in the SEAREX program: an Aerosol Tracer Across the Pacific, in Chemical Oceanography, vol. 10, edited by J. P. Riley and R. Chester, pp. 51-81, Academic, San Diego, Calif., 1989.
- Venrick, E. L., Phytoplankton in an oligotrophic ocean: Observations and questions, Ecol. Monogr., 52, 129-154, 1982.
- Walsh, J. J., On The Nature of Continental Shelves, pp. 1-520, Academic, San Diego, Calif., 1988.

Zhuang, G., R. A. Duce, and D. R. Kester, The dissolution of atmospheric iron in surface seawater of the open ocean, J. Geophys. Res., 95, 16,207-16,215, 1990.

P. R. Betzer, K. L. Carder, D. K. Costello, and R. W. Young, Department of Marine Science, University of South Florida, 140 Seventh Avenue South, Saint Petersburg, FL 33701.

G. R. DiTullio, Moss Landing Marine Laboratories, P. O. Box 450, Moss Landing, CA 95039.

R. A. Duce, J. T. Merrill, and N. W. Tindale, Graduate School of Oceanography, Uni-

versity of Rhode Island, Kingston, RI 02881.

R.A. Feely, Pacific Marine Environmental Laboratory, NOAA, 7600 Sand Point Way NE, Seattle, WA 98115.

E. A. Laws, Department of Oceanography, University of Hawaii, 1000 Pope Road, Honolulu, HI 96822.

M. Uematsu, Department of Marine Sciences and Technology, Hokkaido Tokai University, Minami-sawa, Minami-ku, Sapporo 005, Japan.

(Received September 17, 1990;
revised March 19, 1991;
accepted March 26, 1991.)